

Multi-view Planarity Constraints for Skyline Estimation from UAV Images in City Scale Urban Environments

Ayyappa Swamy Thatavarthy, Tanu Sharma, Harshit Sankhla, Mukul Khanna
and K. Madhava Krishna

Robotics Research Center, International Institute of Information Technology, Hyderabad, India

Keywords: Multi-view Planarity Constraints, Vanishing Lines, PlaneRCNN, Urban Environments, Vision for Aerial Robots.

Abstract: It is critical for aerial robots flying in city scale urban environments to make very quick estimates of a building depth with respect to itself. It should be done in a matter of few views to navigate itself, avoiding collisions with such a towering structure. As such, no one has attacked this problem. We bring together several modules combining deep learning and 3D vision to showcase a quick reconstruction in a few views. We exploit the inherent planar structure in the buildings (facades, windows) for this purpose. We evaluate the efficacy of our pipeline with various constraints and errors from multi-view geometry using ablation studies. We then retrieve the skyline of the buildings in synthetic as well as real-world scenes.

1 INTRODUCTION

Faster navigation of drones, in urban environments, is a challenge as buildings and skyscrapers hinder the long-range capability of on-board cameras. A dense reconstruction of the scene within a few views enables incremental path planning.

Therefore, this paper aims to propose a three stage pipeline as depicted in Figure 1 to reconstruct the skyline of buildings using only 3-5 images of the scene captured by an Unmanned Aerial Vehicle (UAV) or an aerial robot. The three stages are 1) pre-processing of the images, 2) initial estimation of the sparse structure followed by its refinement using a modified bundle adjustment, and 3) retrieval of the skyline of the scene by performing a dense reconstruction.

City scale urban environments are populated by buildings with inherent piecewise planar structures. To leverage these geometric cues, we employ a deep neural architecture, PlaneRCNN proposed by (Liu et al., 2018a), to detect visible planar facades with their segmentation masks in the images.

We then extract the notable features such as line junctions, vanishing points, and vanishing lines from each detected plane mask. Orientation of the plane segments is estimated by computing their normals using their corresponding vanishing lines. The geometric constraints that bind the line junctions to the planes in 3D are deduced from multiple views and are stacked into a single constraints matrix. Solving this matrix's null space gives an initial sparse estimate of

the piecewise planar structure.

This structure is then refined using a modified bundle adjustment step to minimize a combination of residual terms, as explained in section 3. The facade masks are then projected onto the refined sparse structure to obtain a dense reconstruction. Skyline of the buildings is then retrieved using the dense reconstruction.

Our contributions are:

- a pipeline with several modules combining deep learning and 3D vision to showcase a quick reconstruction of the skyline within a few views.
- a novel way of assimilating different geometric constraints from multiple views for simultaneous initialization of multiple planar structures.
- a study of the efficacy of various structural/geometric constraints, nascent to the 3D vision literature, on initialization, and bundle adjustment.

The paper is organized as follows. In section 2, we list the works related to the current approach, and in section 3, the methodology of our pipeline is presented. The results of our experiments are described in section 4, followed by conclusions in section 5.

2 RELATED WORK

Reconstructing 3D geometry of an urban scene within a few views from UAV images is not a well-studied

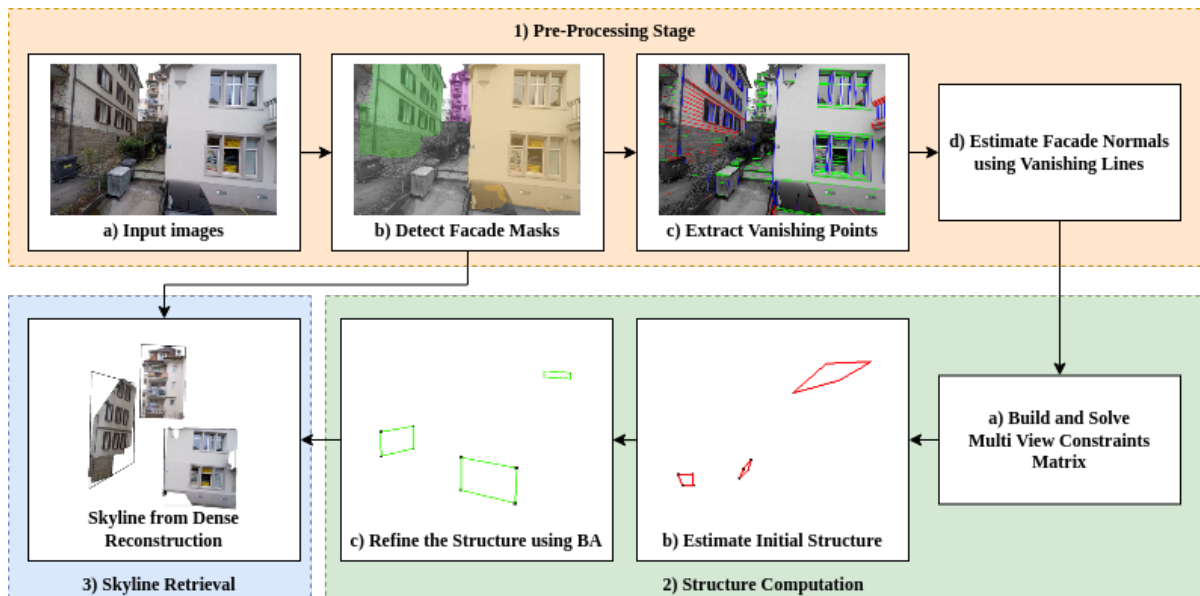


Figure 1: Overall pipeline of the proposed method. First four steps (in the top row) are part of the pre-processing stage (1). The next three steps (from right of bottom row) form the structure computation stage (2). And the last step represents the skyline retrieval stage (3). Images in each step represents the results obtained real world UrbanMAV dataset introduced by (Majdik et al., 2017). Step 1(b) shows the segmentation masks of the planar facades generated by PlaneRCNN. Step 1(c) shows the line segments on the detected facades coloured by their vanishing point directions. Step 2(b) shows the initial estimate of the 3D line junctions. Step 2(c) shows the refined 3D structure after bundle adjustment using various geometric constraints. Step 3 shows the dense reconstruction and the retrieved skyline (black border surrounding each facade).

problem in Computer Vision literature.

Some methods (Zhou et al., 2017) use deep neural network architectures to predict depth and motion from videos simultaneously. SLAM methods like (Li et al., 2018), PL-SLAM(Gomez-Ojeda et al., 2019) only focus on landmarks for localization and mapping. These landmarks are usually sparse and not very useful for estimating the skylines in outdoor environments. They also require a good set of features to track and initialize their system.

While there are many methods for detecting and recovering building structures from aerial and satellite images, approaches that reconstruct using low altitude images are difficult to find in the literature.

For facade detection and segmentation from images, (Akbulut et al., 2018) have used LiDAR data.

There are a few learning based frameworks like PlaneNet (Liu et al., 2018b), PlaneRecover (Yang and Zhou, 2018) and PlaneRCNN (Liu et al., 2018a) to detect planes from 2D images. Both PlaneNet and PlaneRecover have a limitation on the number of planes detected 10 and 5, respectively. We use PlaneRCNN for plane segmentation, as it uses a detection network to overcome this limitation.

Most of the existing methods estimate the layout of an urban scene from a single 2D image. These are not directly useful to build a meaningful local map

useful for path planning and navigation. Some of the single view based approaches that work in outdoor urban scenes are as follows. (Zhou et al., 2019) have proposed a method to recover 3D wireframe from single view images. Some other methods like (Ramalingam and Brand, 2013) and (Ranade and Ramalingam, 2018) use vanishing points and lines to lift the 2D features to 3D by imposing geometric constraints.

(Straub et al., 2018) have proposed the notion of the Manhattan-Frame (MF) model to formalize the surface normals of orthogonal and parallel planar structures in man-made environments. Given a set of surface normals or vanishing points, (Joo et al., 2019) estimate the MF in near real-time and apply it to estimate multiple MFs. In general, a manhattan scene is described by two mutually perpendicular vanishing points and a vertical vanishing point. To model more complex urban scenes, (Schindler and Dellaert, 2004) have proposed Atlanta World with more than two horizontal vanishing point directions. (Li et al., 2019) have used Atlanta World based constraints to improve line based SLAM.

(Khurana et al., 2012) proposed geometric constraints for single-view reconstruction of buildings with a user-guided interface. To avoid the depth ambiguity due to projective single view geometry, they also assume that a reference plane such as the ground

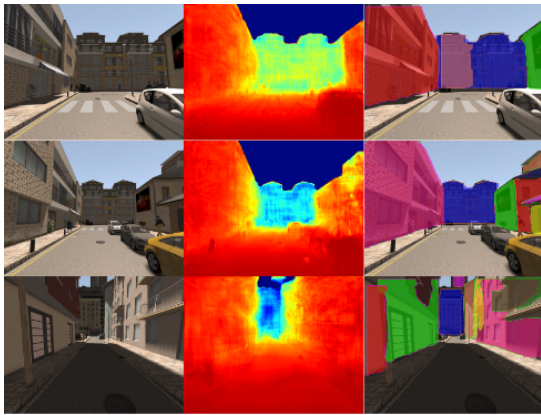


Figure 2: Results on test images after fine-tuning PlaneRCNN on SYNTHIA dataset.

or one of the building facades is reconstructed in 3D. This assumption cannot be made when reconstructing the buildings in real-time.

In contrast, we consider 3 to 5 images per scene for reconstruction. Instead of a user-guided interface, we use PlaneRCNN to automatically segment the individual planar facades of buildings in the scene. We then utilize the information from nearby views in the form of various planar constraints to avoid the need for a reference plane.

3 METHODOLOGY

3.1 Pipeline

The steps involved in the proposed pipeline are described as follows:

- Preprocessing of UAV images
- Initialization and refinement of sparse structure using geometric constraints
- Dense reconstruction followed by skyline retrieval

3.2 Pre-processing

Each image in the sequence is pre-processed using the steps depicted in Figure 1. Each step is described in the following sections.

3.2.1 Facade Detection

In urban scenes, skyline is formed by planar facades of buildings. For computational purposes, the facades can be assumed to be planes in 3D.

To predict the facades/plane segment instances of buildings, we have trained PlaneRCNN on SYNTHIA dataset.

The architecture of PlaneRCNN is briefly described as follows. It uses Mask R-CNN (He et al., 2017) as its backbone to detect planar and non-planar regions, where each planar region is considered an object instance. Besides this, it contains two modules viz., segmentation refinement network, and warping loss module.

The segmentation refinement module jointly optimizes all the detected masks by comparing them using a cross-entropy loss. Its U-Net architecture (Ronneberger et al., 2015) uses ConvAccu modules, which are based on non-local modules (Wang et al., 2017).

The warping loss module enforces the consistency of reconstructed 3D planes with a nearby view during the training. The 3D points p_n of a nearby view are projected on the current view, and current view coordinates p_c are read using bilinear interpolation. Then, p_c are transformed to nearby coordinate frame p'_c to compute the L2 norm between p'_c and p_n .

PlaneRCNN detects plane instances, predicts plane parameters, and per-pixel depthmap. However, we have observed that discontinuities like balconies, protrusions, and depression on the building walls lead to a poor prediction of plane normals and depth map. So, we limit its usage to predict plane segment masks.

3.2.2 Normal Estimation

Each facade contains a horizontal and a vertical vanishing point. A line joining any two vanishing points is called a Vanishing Line. Normal (\mathbf{n}) of the facade plane can be computed using vanishing line (l_v) using the formula:

$$\mathbf{n} = \mathbf{R}^T (\mathbf{K}^T l_v) \quad (1)$$

where \mathbf{R} and \mathbf{K} represent the rotation and camera calibration matrices respectively.

LSD algorithm, as mentioned in (Grompone von Gioi et al., 2012) is used to extract the line segments within the facade segment in the image. Vanishing points are computed and are assigned to the line segments using the approach described in (Lezama et al., 2017).

3.3 Initialization

Buildings can be reconstructed by considering the piece-wise planar surfaces of the facades. To achieve that, a 2D polygon (formed by joining the line junctions) is detected on the facade's image and tracked across neighbouring views. We use this information

$$\begin{pmatrix}
 l_1^{jT} \mathbf{P}^j & 0 & 0 & 0 & l_1^{jT} \mathbf{p}_4^j \\
 0 & l_1^{jT} \mathbf{P}^j & 0 & 0 & l_1^{jT} \mathbf{p}_4^j \\
 0 & l_2^{jT} \mathbf{P}^j & 0 & 0 & l_2^{jT} \mathbf{p}_4^j \\
 0 & 0 & l_2^{jT} \mathbf{P}^j & 0 & l_2^{jT} \mathbf{p}_4^j \\
 0 & 0 & l_3^{jT} \mathbf{P}^j & 0 & l_3^{jT} \mathbf{p}_4^j \\
 0 & 0 & 0 & l_3^{jT} \mathbf{P}^j & l_3^{jT} \mathbf{p}_4^j \\
 0 & 0 & 0 & l_4^{jT} \mathbf{P}^j & l_4^{jT} \mathbf{p}_4^j \\
 l_4^{jT} \mathbf{P}^j & 0 & 0 & 0 & l_4^{jT} \mathbf{p}_4^j \\
 \mathbf{t}_x^{1j} & 0 & 0 & 0 & l_{4x}^{1j} \\
 \mathbf{t}_y^{1j} & 0 & 0 & 0 & l_{4y}^{1j} \\
 0 & \mathbf{t}_x^{2j} & 0 & 0 & l_{4x}^{2j} \\
 0 & \mathbf{t}_y^{2j} & 0 & 0 & l_{4y}^{2j} \\
 0 & 0 & \mathbf{t}_x^{3j} & 0 & l_{4x}^{3j} \\
 0 & 0 & \mathbf{t}_y^{3j} & 0 & l_{4y}^{3j} \\
 0 & 0 & 0 & \mathbf{t}_x^{4j} & l_{4x}^{4j} \\
 0 & 0 & 0 & \mathbf{t}_y^{4j} & l_{4y}^{4j} \\
 \mathbf{n}^j & -\mathbf{n}^j & 0 & 0 & 0 \\
 0 & \mathbf{n}^j & -\mathbf{n}^j & 0 & 0 \\
 0 & 0 & \mathbf{n}^j & -\mathbf{n}^j & 0 \\
 \mathbf{n}^j & 0 & 0 & -\mathbf{n}^j & 0
 \end{pmatrix}
 \begin{pmatrix}
 \mathbf{V}_1 \\
 \mathbf{V}_2 \\
 \mathbf{V}_3 \\
 \mathbf{V}_4 \\
 1
 \end{pmatrix}
 = 0$$

Figure 3: A sample constraints matrix built from j^{th} view of a 3D quadrilateral defined by the vertices $\mathbf{V}_1, \mathbf{V}_2, \mathbf{V}_3$ and \mathbf{V}_4 . \mathbf{P}^j represents the projection matrix of j^{th} view. \mathbf{t}_x and \mathbf{t}_y represent the standard point triangulation constraints. \mathbf{n}^j represents the normal of the plane computed using the equation (1). First eight rows of the matrix represent frustum constraints. Next eight rows are from the triangulation constraints. The last four rows arise from the orientation/normal constraints.

along with standard triangulation to build a multi-view constraints matrix. This matrix's null space is found using SVD (Singular Value Decomposition) to get an initial algebraic estimate of the structure. To minimize the residual errors in the initial estimate, another step of least-squares minimization is performed, which serves as the initialization for the 3D structure (depicted by red polygons in Fig 1).

At this stage, the 3D structure represents approximate positions of vertices of the 3D polygons on buildings' facades.

In the bundle adjustment stage (explained in the next section), different combinations of planar constraints are imposed besides the standard reprojection error (E_r). The constraints ensure that the vertices and the poses are simultaneously optimized while maintaining geometric consistency.

Frustum Constraint.

A 3D polygon is represented by a list of vertices:

$$\begin{aligned}
 \mathbf{V}_1 &= (V_{1x}, V_{1y}, V_{1z})^T \\
 \mathbf{V}_2 &= (V_{2x}, V_{2y}, V_{2z})^T \\
 &\dots
 \end{aligned}$$

and so forth.

The edges of the polygon in the image may be denoted as l_1, l_2, \dots, l_s . If an edge i is projected from the center of the camera, it sweeps a plane in 3D.

The volume bounded by the planes formed by each edge of the polygon is defined as a frustum.

As each vertex of an s -sided polygon lies on the two intersecting edges, s vertices give rise to $2s$ frustum constraints from each view. If the polygon is visible in n views, each polygon gives rise to $2sn$ frustum constraints:

For a vertex $\tilde{\mathbf{V}}_j$ (where $\tilde{\mathbf{V}}_j$ represents homogenous coordinates) of an i^{th} quadrilateral visible in n views, the following equation represents the $2n$ frustum constraints.

$$\begin{aligned}
 (\mathbf{P}^{1T} l_{1i}^1)^T \tilde{\mathbf{V}}_j &= 0 \\
 (\mathbf{P}^{1T} l_{2i}^1)^T \tilde{\mathbf{V}}_j &= 0 \\
 &\vdots \\
 (\mathbf{P}^{nT} l_{1i}^n)^T \tilde{\mathbf{V}}_j &= 0 \\
 (\mathbf{P}^{nT} l_{2i}^n)^T \tilde{\mathbf{V}}_j &= 0
 \end{aligned}$$

where j represents all vertices lying on edge i .

The error term representing the frustum constraint, in general, can be defined as:

$$e_f = \|(\mathbf{P}^T l) \tilde{\mathbf{V}}_j\|_2 \quad (2)$$

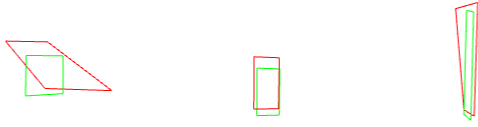


Figure 4: Results of the sparse structure before and after the modified bundle adjustment. Red polygons represent the estimate of the structure on a SYNTHIA sequence before the bundle adjustment step. Green polygons represent the refined structure after bundle adjustment using all the combinations of constraints mentioned in the section 3.3.

Orientation Constraint.

The normals of each facade are computed from the vanishing lines. Its error term can be represented as follows :

$$e_o = \|\mathbf{n}^T \cdot (\mathbf{V}_2 - \mathbf{V}_1)\|_2 \quad (3)$$

Scalar Triple Product (STP).

Scalar Triple Product represents the volume of a parallelepiped. The scalar triple product of four points in 3D is zero if they are coplanar. It is computed using the 3D vertices:

$$e_s = (\mathbf{V}_3 - \mathbf{V}_1) \cdot [(\mathbf{V}_2 - \mathbf{V}_1) \times (\mathbf{V}_4 - \mathbf{V}_1)] \quad (4)$$

Manhattan Constraint.

Based on their normals, facades are assigned one of the two horizontal vanishing directions. As they are orthogonal to each other, the Manhattan constraint is defined as:

$$e_m = \mathbf{n}_1^T \cdot \mathbf{n}_2 \quad (5)$$

Multi-view Constraints Matrix.

It is to be noted that the Triangulation, Frustum, and Orientation constraints are linear in terms of the 3D vertices. So, a combination of these three constraints is used to build the multi-view constraints matrix shown in Figure (3).

As it captures the constraints of all the 3D quadrilaterals obtained from all views, it is used to get a one-shot initialization of the all the piecewise planar structures in the scene.

As this is in the form $\mathbf{AX} = \mathbf{0}$, its null space (containing the vertices) is solved using SVD. This gives the initial algebraic estimate of the structure.

3.4 Modified Bundle Adjustment

So far, the vertices obtained may not lie on a plane, thereby deforming the planar structure of the facades of the building. To overcome this, we modify bundle



(a)



(b)

Figure 5: a) Image of a real-world building captured by an RGB camera mounted on a UAV. b) shows a novel view of the dense reconstruction obtained with our method using only 5 views of the scene.

adjustment to simultaneously optimize for the planar structure and the poses using different combinations of residual terms besides the reprojection error. The residuals are computed from the parameters viz., initialized 3D vertices, and the poses.

Total Residual.

The total residual is computed as the weighted sum of all the constraints involved in the combination.

$$e = e_r + e_f + e_o + e_m + e_s \quad (6)$$

Figure 4 shows the results of the structure before and after the bundle adjustment.

3.5 Skyline Retrieval

The plane parameters of each facade are computed from the refined structure. All pixels that lie inside the facade masks are then projected onto their respective

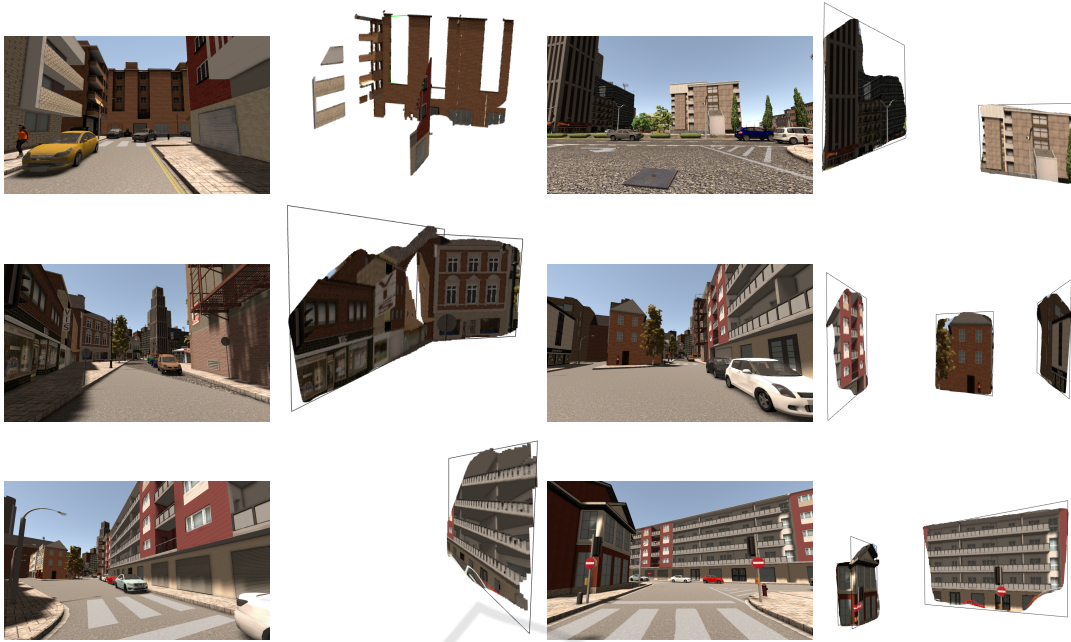


Figure 6: Qualitative results obtained on photo-realistic views from SYNTHIA dataset. Only 3-5 images per scene are considered. Skylines of the buildings retrieved using our method from 6 different scenes are shown. Dense reconstruction is visualized using Open 3D (Zhou et al., 2018) software.

Table 1: Ablation study on contributions of two components in PlaneRCNN. VOI, RI and SC are the metrics with abbreviations Variation Of Information, Rand Index and Segmentation Covering respectively. Plane segmentation metrics are computed on the SYNTHIA dataset.

Method	VOI ↓	RI ↑	SC ↑
warping + refine (pre-trained)	2.556	0.536	0.376
warping + refine (re-trained on SYNTHIA)	1.495	0.793	0.677
refine (re-trained on SYNTHIA)	1.222	0.863	0.770

Table 2: Various errors (averaged across the test scenes) in the initial estimates of the structure after the stages 2a and 2b. This shows the improvement in structure due to least squares minimization or geometric correction (stage 2b) on the initial estimate obtained algebraically using SVD of the multi-view constraints matrix (stage 2a).

Stage of initialization	Plane Orientation (deg)	Depth (cm)	Coplanarity (cm ³)	Manhattan (deg)
2a	18.183	14.227	0.935	31.798
2b	11.079	13.825	0.697	31.244

Table 3: Ablation study of imposing various structural constraints on BA (stage 2c of Figure 1), showing the overall improvement in the structure. The errors are computed using the ground truth of SYNTHIA dataset (Averaged across the test scenes).

Constraints	Plane Orientation (deg)	Depth (cm)	Coplanarity (cm ³)	Manhattan (deg)
e_r	10.824	12.884	1.093	30.905
$e_r + e_s$	10.545	12.737	1.042	30.793
$e_r + e_s + e_f$	10.075	52.522	1.269	33.121
$e_r + e_s + e_f + e_m$	9.781	21.799	0.903	29.156

reconstructed planes to generate a dense reconstruction of the plane segment. Thus the skyline is drawn along the border of the plane segment.

4 EXPERIMENTS AND RESULTS

We have evaluated the proposed pipeline on different scenes of SYNTHIA as well as UrbanMAV datasets.

We have used PlaneRCNN (Liu et al., 2018a) framework for building facade/plane segmentation.

Originally, PlaneRCNN is trained on the ScanNet (Dai et al., 2017), an indoor dataset. This resulted in poor predictions when using the pre-trained model SYNTHIA (Ros et al., 2016), which is an outdoor dataset. Two problems were identified with the pre-trained model detections - 1) Only planes near the camera were detected, and 2) It detected planes of other objects like cars, which are not required. As shown in Figure(2), re-training the network on SYNTHIA resulted in better mask predictions. The re-trained model is able detect far-off and very small planes while ignoring unnecessary planes like the ground, car roof, car doors, etc.

We have trained PlaneRCNN on 1018 images of the Synthia-SUMMER-04 sequence for ten epochs with a learning rate of $1e^{-4}$ on an NVIDIA GTX 1080 Ti GPU. SYNTHIA dataset does not have plane instance segmentation. So, the dataset was manually annotated with plane instances. We have observed that, PlaneRCNN with the segmentation refinement module gives a better result than with both the refinement and the warping module in detecting the plane segments on the facades of buildings. We have evaluated plane segmentation quality for the pre-trained model and trained model (using different modules) on the SYNTHIA dataset (tabulated in Table 2). The metrics used are - variation of information (VOI), Rand index (RI), and segmentation covering (SC) (Yang and Zhou, 2018).

Variation of Information (VOI) metric is used for clustering comparison. It measures the distance between two segmentations in terms of their average conditional entropy and is given by

$$VOI(S, S') = H(S) + H(S') - 2I(S, S') \quad (7)$$

where, H and I represent, respectively, entropies and mutual information between two clusterings of data S and S' . Less similar the two segmentations, higher is the VOI.

Rand Index allows the comparison of a test segmentation with multiple ground-truth segmentations through soft nonuniform weighting of pixel pairs as a function of the variability in the ground-truth set.

$$RI(S, \{G_k\}) = \frac{1}{T} \sum_{i < j} [c_{ij} p_{ij} + (1 - c_{ij})(1 - p_{ij})] \quad (8)$$

where, $\{G_k\}$ is the set of ground-truth segmentations, c_{ij} is the event that pixels i and j have same label and p_{ij} is its probability and T is total number of pixel pairs.

Segmentation Covering (SC) of a segmentation S by a segmentation S' is defined as

$$C(S' \rightarrow S) = \frac{1}{N} \sum_{R \in S} |R| \cdot \max_{R' \in S'} O(R, R') \quad (9)$$

where,

$$O(R, R') = \frac{|R \cap R'|}{|R \cup R'|} \quad (10)$$

and N denotes total number of pixels in the image. Similarly, the covering of a machine segmentation S by a family of ground-truth segmentations $\{G_i\}$ is defined by first covering S separately with each human segmentation G_i and then averaging over the different humans. To achieve perfect covering, the machine segmentation must explain all of the human data. We can then define two quality descriptors for regions: the covering of S by $\{G_i\}$ and the covering of $\{G_i\}$ by S .

We have used C++ based optimization library `ceres-solver`(Agarwal et al.,) for initialization and bundle adjustment steps.

Figure (5b) shows the reconstruction of a real-world building captured from a UAV obtained using our proposed method. The UAV used is equipped with an mvBlueFOX monocular camera with a resolution of 1.3MP. Five images of the scene have been used to reconstruct the scene using the proposed pipeline.

Figure (6) shows the qualitative results with the dense reconstructions and skylines obtained by following our method.

Quantitative results obtained on the synthetic dataset (SYNTHIA) only are reported in tables 2 & 3, as the ground truth depth maps are unavailable on real world UrbanMAV dataset. The error metrics are computed by comparing the estimated vertices against the vertices obtained from ground truth depth. The values are presented in (cm) to show the accuracy of the method when evaluated in synthetic scenes. Plane Orientation and Manhattan errors depicts the average deviation of the normals of the planes in scene w.r.t the ground truth plane normals. Table 2 shows the advantage of using stage 2b to improve the initial algebraic estimate. Table 3 shows the improvement in the structure after the bundle adjustment modified by imposing various constraints. As the orientation residual term (e_o) in BA is computed using the normals computed from the vanishing line, it is sensitive to the errors in the line feature detection. As this resulted in increase of the error metrics after the BA stage, it is not reported in Table 3. Nonetheless, the Orientation constraint in the stages 2a and 2b, proved to be useful in reducing the plane normal deviation of estimated structure.

5 CONCLUSION

In this paper, we have shown that using the constraints have improved the depth and orientation estimates of piecewise planar structures in city scale urban environments.

By training PlaneRCNN to detect the buildings' planar facades, the geometric information of each visible facade can be extracted. Imposing the deduced multi-view geometric constraints by modifying the standard bundle adjustment resulted in improved depth and orientation estimates. The dense reconstruction of the facades is obtained by using the facade masks generated by the neural network. In some cases, the increase in depth error has been compensated by the decrease of orientation error, ensuring structural improvement.

The skyline, thus retrieved from the dense reconstruction, can be used in navigation and path planning.

ACKNOWLEDGEMENTS

We thank Shivaan Sehgal and Sidhant Subramanian, for annotating the building facades in SYNTHIA dataset and Mukul Khanna, for helping out with facade detection network experiments. We also thank Krishna Murthy J. at Real and Embodied AI Lab, Université de Montréal for valuable feedback/advice during the brainstorming sessions.

REFERENCES

- Agarwal, S., Mierle, K., and Others. Ceres solver. <http://ceres-solver.org>.
- Akbulut, Z., Özdemir, S., Acar, H., and Karsli, F. (2018). Automatic building extraction from image and lidar data with active contour segmentation. *Journal of the Indian Society of Remote Sensing*, 46(12):2057–2068.
- Dai, A., Chang, A. X., Savva, M., Halber, M., Funkhouser, T., and Nießner, M. (2017). Scannet: Richly-annotated 3d reconstructions of indoor scenes.
- Gomez-Ojeda, R., Moreno, F., Zuñiga-Noël, D., Scaramuzza, D., and Gonzalez-Jimenez, J. (2019). Pl-slam: A stereo slam system through the combination of points and line segments. *IEEE Transactions on Robotics*, 35(3):734–746.
- Grompone von Gioi, R., Jakubowicz, J., Morel, J.-M., and Randall, G. (2012). LSD: a Line Segment Detector. *Image Processing On Line*, 2:35–55.
- He, K., Gkioxari, G., Dollár, P., and Girshick, R. (2017). Mask r-cnn.
- Joo, K., Oh, T., Kim, J., and Kweon, I. S. (2019). Robust and globally optimal manhattan frame estimation in near real time. *IEEE Transactions on Pattern Analysis and Machine Intelligence*, 41(3):682–696.
- Khurana, D., Sankhla, S., Shukla, A., Varshney, R., Kalra, P., and Banerjee, S. (2012). A grammar-based gui for single view reconstruction. In *Proceedings of the Eighth Indian Conference on Computer Vision, Graphics and Image Processing, ICVGIP '12*, New York, NY, USA. Association for Computing Machinery.
- Lezama, J., Randall, G., and Grompone von Gioi, R. (2017). Vanishing Point Detection in Urban Scenes Using Point Alignments. *Image Processing On Line*, 7:131–164.
- Li, H., Xing, Y., Zhao, J., Bazin, J., Liu, Z., and Liu, Y. (2019). Leveraging structural regularity of atlanta world for monocular slam. In *2019 International Conference on Robotics and Automation (ICRA)*, pages 2412–2418.
- Li, H., Yao, J., Bazin, J., Lu, X., Xing, Y., and Liu, K. (2018). A monocular slam system leveraging structural regularity in manhattan world. In *2018 IEEE International Conference on Robotics and Automation (ICRA)*, pages 2518–2525.
- Liu, C., Kim, K., Gu, J., Furukawa, Y., and Kautz, J. (2018a). Planercnn: 3d plane detection and reconstruction from a single image.
- Liu, C., Yang, J., Ceylan, D., Yumer, E., and Furukawa, Y. (2018b). Planenet: Piece-wise planar reconstruction from a single rgb image.
- Majdik, A. L., Till, C., and Scaramuzza, D. (2017). The Zurich urban micro aerial vehicle dataset. *The International Journal of Robotics Research*, 36(3):269–273.
- Ramalingam, S. and Brand, M. (2013). Lifting 3d manhattan lines from a single image. In *2013 IEEE International Conference on Computer Vision*, pages 497–504.
- Ranade, S. and Ramalingam, S. (2018). Novel single view constraints for manhattan 3d line reconstruction. In *2018 International Conference on 3D Vision (3DV)*, pages 625–633.
- Ronneberger, O., Fischer, P., and Brox, T. (2015). U-net: Convolutional networks for biomedical image segmentation.
- Ros, G., Sellart, L., Materzynska, J., Vazquez, D., and Lopez, A. M. (2016). The SYNTHIA Dataset: A Large Collection of Synthetic Images for Semantic Segmentation of Urban Scenes. In *2016 IEEE Conference on Computer Vision and Pattern Recognition (CVPR)*, pages 3234–3243, Las Vegas, NV, USA. IEEE.
- Schindler, G. and Dellaert, F. (2004). Atlanta world: an expectation maximization framework for simultaneous low-level edge grouping and camera calibration in complex man-made environments. In *Proceedings of the 2004 IEEE Computer Society Conference on Computer Vision and Pattern Recognition, 2004. CVPR 2004.*, volume 1, pages I–I.
- Straub, J., Freifeld, O., Rosman, G., Leonard, J. J., and Fisher, J. W. (2018). The manhattan frame

- model—manhattan world inference in the space of surface normals. *IEEE Transactions on Pattern Analysis and Machine Intelligence*, 40(1):235–249.
- Wang, X., Girshick, R., Gupta, A., and He, K. (2017). Non-local neural networks.
- Yang, F. and Zhou, Z. (2018). Recovering 3d planes from a single image via convolutional neural networks.
- Zhou, Q.-Y., Park, J., and Koltun, V. (2018). Open3D: A modern library for 3D data processing. *arXiv:1801.09847*.
- Zhou, T., Brown, M., Snavely, N., and Lowe, D. G. (2017). Unsupervised learning of depth and ego-motion from video. In *2017 IEEE Conference on Computer Vision and Pattern Recognition (CVPR)*, pages 6612–6619.
- Zhou, Y., Qi, H., Zhai, Y., Sun, Q., Chen, Z., Wei, L.-Y., and Ma, Y. (2019). Learning to Reconstruct 3D Manhattan Wireframes from a Single Image. *arXiv:1905.07482 [cs]*. arXiv: 1905.07482.

